

Three-dimensional smoothed particle hydrodynamics modeling of preferential flow dynamics at fracture intersections on a high-performance computing platform

Lysander Bresinsky¹ and Jannes Kordilla¹

¹University of Göttingen, Geoscientific Centre, Göttingen, Germany

November 23, 2022

Abstract

The physical mechanisms that govern preferential flow dynamics in unsaturated fractured rock formations are complex and not well understood. Fracture intersections are critical relay points along preferential flow paths and control the partitioning behavior, leading to temporal delay and intermittent flow. In this work, a three-dimensional Pairwise-Force Smoothed Particle Hydrodynamics (PF-SPH) model is being applied in order to simulate gravity-driven droplet flow at synthetic fracture intersections. SPH, as a mesh-less Lagrangian method, is particularly suitable for modeling deformable interfaces, such as three-phase contact dynamics of droplets. The static and dynamic contact angle can be recognized as the most important parameter of gravity-driven free-surface flow. In SPH, surface tension and adhesion naturally emerges from the implemented pairwise fluid-fluid (s-f f) and solid-fluid (s-sf) interaction force. The model was calibrated to a contact angle of 65° , which corresponds to the wetting properties of water on Poly(methyl methacrylate). The accuracy of the SPH simulations were validated against an analytical solution of Poiseuille flow between two parallel plates and against laboratory experiments. Using the SPH model, the complex flow mode transitions from droplet to rivulet flow of an experimental study were reproduced. Additionally, laboratory dimensionless scaling experiments of water droplets were successfully replicated in SPH. Finally, SPH simulations were used to investigate the partitioning dynamics of single droplets into synthetic horizontal fractures with various apertures ([?]d_f = 0, 0.5, 1.0, 1.5, 2.0, 2.5, 3.0, 3.5, 4.0 mm) and offsets ([?]d_of f = 1.5, 1.0, 0.5, 0, 1.0, 2.0, 3.0 mm). The perfect conditions of ideally smooth surfaces and the SPH inherent advantage of particle tracking allow the recognition of small scale partitioning mechanisms and its importance for bulk flow behavior. The aim of this study is to derive an analytical correlation and interpretation of partitioning dynamics, droplet height and aperture

Three-dimensional smoothed particle hydrodynamics modeling of preferential flow dynamics at fracture intersections on a high-performance computing platform

I. Introduction

Free-surface flow at fracture intersections

- Fracture intersections are critical relay points along preferential flow paths and control the partitioning (i.e. dispersion) behavior in fractured porous media
- Highly non-linear and rapid flow processes such as droplets, rivulets and (adsorbed) films affect the bypass dynamics at fracture intersections (Kordilla, 2017)
- Volume-averaged models (e.g. Richards equation) with saturation-capillary-pressure relations (e.g. van Genuchten parameterization) do not account for complex flow mechanisms on a fracture- and fracture-network-scale
- Flows in unsaturated fractures are challenging to study numerically due to the presence of complex air-water interfaces

Key Objectives:

- Develop a better understanding of the controlling factor of fracture intersections towards droplet partitioning and its implications for preferential flow
- Link geometric fracture characteristics and fluid properties to determine bypass efficiency and transition thresholds
- Analytical interpretation of the controlling factors

II. Methods

SPH implementation of the Navier-Stokes equation

- The foundations of SPH rely on the Navier-Stokes equations:

$$\frac{d\mathbf{v}}{dt} = -\frac{1}{\rho}\nabla p + \frac{\mu}{\rho}\nabla^2\mathbf{v} + \mathbf{g} \quad (1)$$

- Rewritten in SPH form:

$$\frac{d\mathbf{v}_i}{dt} = -\sum_{j \in f+s} m_j \left(\frac{p_j}{\rho_j^2} + \frac{p_i}{\rho_i^2} \right) \mathbf{e}_{ij} \frac{dW(\mathbf{r}_{ij}, h)}{dr_{ij}} + 2\mu \sum_{j \in f+fluid} m_j \frac{\mathbf{v}_{ij}}{\rho_i \rho_j r_{ij}} \frac{dW(\mathbf{r}_{ij}, h)}{dr_{ij}} + \mathbf{g}_{sph} + \frac{1}{m_i} \sum_{j=1}^N \mathbf{F}_{ij} + \mathbf{f}_i(\mathbf{r}_i, \mathbf{v}_i) \frac{m_k}{\rho_i \rho_k} (\mathbf{n}_i + \mathbf{n}_k) \cdot \frac{dW(\mathbf{r}_{ik}, h)}{dr_{ik}} \quad (2)$$

\mathbf{v}_i : particle velocity t : time p : pressure of particle i m : particle mass
 ρ : mass density \mathbf{r} : position vector h : weighting function range W : weighting function
 \mathbf{g} : gravitation \mathbf{F} : particle interaction force \mathbf{f}_i : volumetric source term \mathbf{n} : normals of the interface
 \mathbf{e}_{ij} : unit vector

- In the above equation the linearized viscosity term acts in between fluid particles only
- The interaction force is defined following Tartakovsky (2005) and Kordilla (2017) as a cubic-spline type function with short-range repulsive and long-range attractive components
- The variable slip boundary condition is imposed according to Pan (2014) via a volumetric source term $\mathbf{f}_i = \beta \mathbf{v}$, where \mathbf{n} are the respective normals of the solid-fluid interface
- $\beta = 0$ (full slip) and $\beta = \infty$ (no-slip)
- Here β is chosen such that no-slip conditions are enforced
- Pressure is obtained from an equations of state (EOS)

$$p_i = \epsilon \left(\frac{\rho_i}{\rho_0} \right)^\Gamma + p_0, \quad (3)$$

ρ_0 : rest density p_0 : background pressure ϵ : scaling constant

- Density is obtained from a kernel summation

$$\rho_i = \int_{j=1}^N m_j W(\mathbf{r}_{ij}, h) \quad (4)$$

- Interparticle forces F_{ij} generate cohesion and adhesion

$$\mathbf{F}_{ij} = \begin{cases} s \cdot \cos\left(\frac{1.5\pi}{3\alpha} |\mathbf{r}_{jil}|\right) \frac{\mathbf{r}_{ji}}{|\mathbf{r}_{ji}|} & \text{for } |\mathbf{r}_{jil}| \leq h \\ 0 & \text{for } |\mathbf{r}_{jil}| > h \end{cases} \quad (5)$$

s : interaction strength that can either describe solid-fluid s_{sf} or fluid-fluid interactions s_{ff}

III. Model calibration

- The static and dynamic contact angle control gravity-driven free-surface flow
- Critical calibration parameters: (a) fluid-fluid s_{ff} , (b) solid-fluid s_{sf} interaction strength, (c) speed of sound c_0 and (d) friction coefficient β

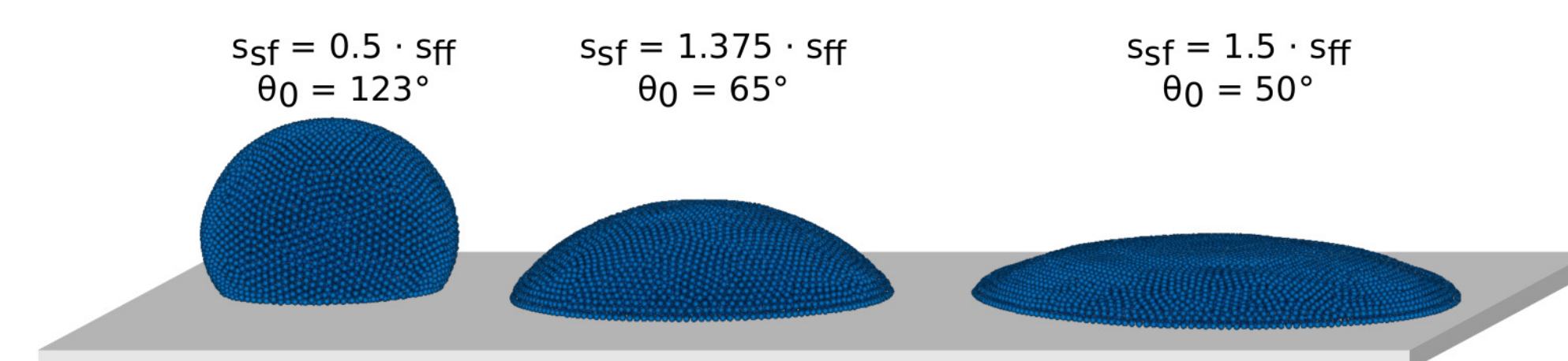


Figure 1: Contact angles formed by sessile droplets in SPH.

Surface tension

- Cohesive forces naturally created by s_{ff} and the EOS
- Young-Laplace Law

$$\sigma = \frac{R_{eq} \Delta P}{2} \quad (6)$$

R_{eq} : radius at equilibrium σ : surface tension
 ΔP : pressure difference

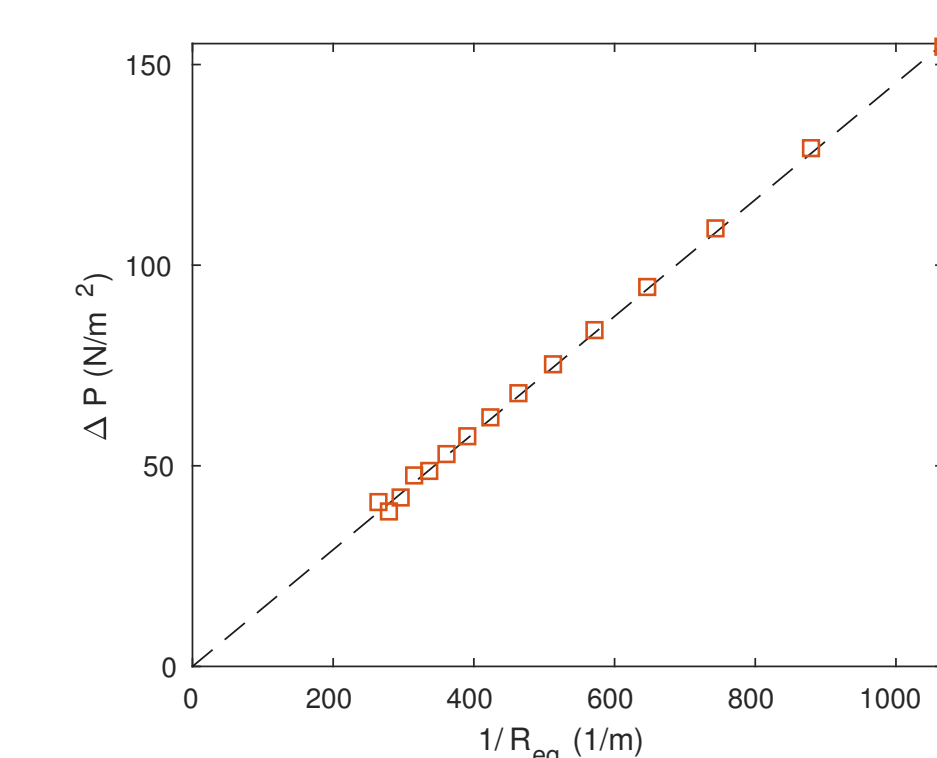


Figure 2: Pressure gradient ΔP of a simulated droplet under zero gravity

Static contact angle

- Utilized to implement different wetting characteristics (fig. 1)
- Droplets on acrylic glass matching goniometer measurements ($\sigma = 65^\circ$)

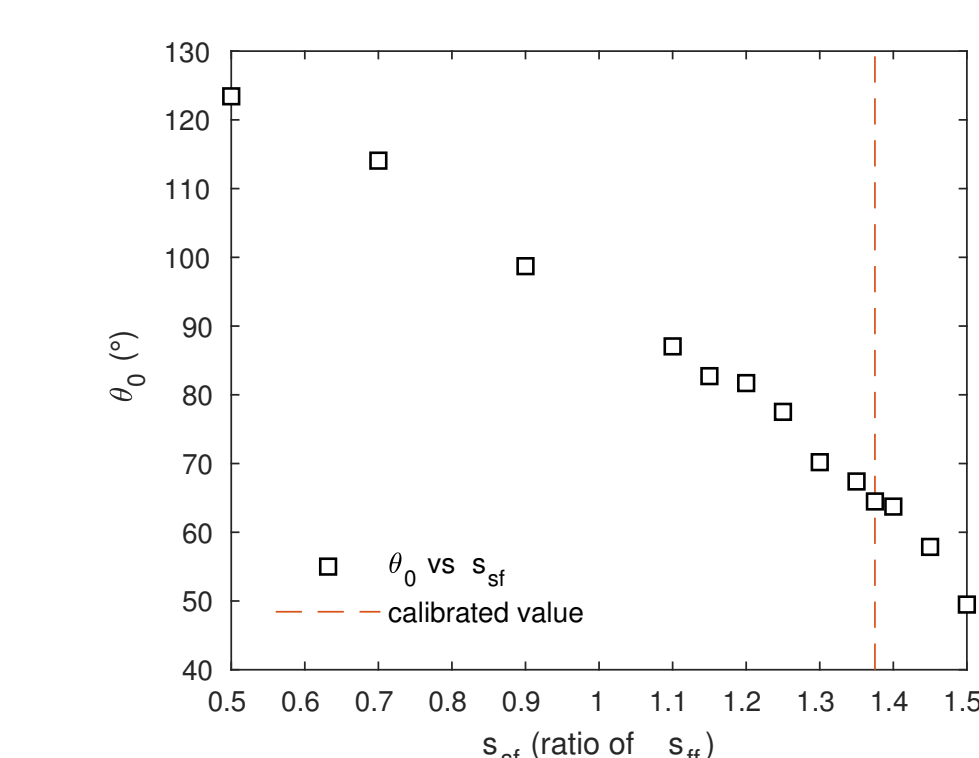


Figure 3: Numerical dependence of static contact angle θ_0 and s_{sf}

IV. Single-inlet partitioning dynamics

Model geometry

- Adjustment of aperture d_f and offset d_{off} by shifting the lower cube (fig. 4).
- Fluid masses are measured in the domains R_1 , R_2 and R_3 .

General observations

- Small droplets may not overcome discontinuities (Fig. 5a)
- Medium sized droplets get fully trapped in horizontal fracture (Fig. 5b)

- Large droplets have a more focused and enhanced momentum, allowing the droplet to hydraulically connect to the lower horizontal fracture wall (Fig. 5c,d,e)

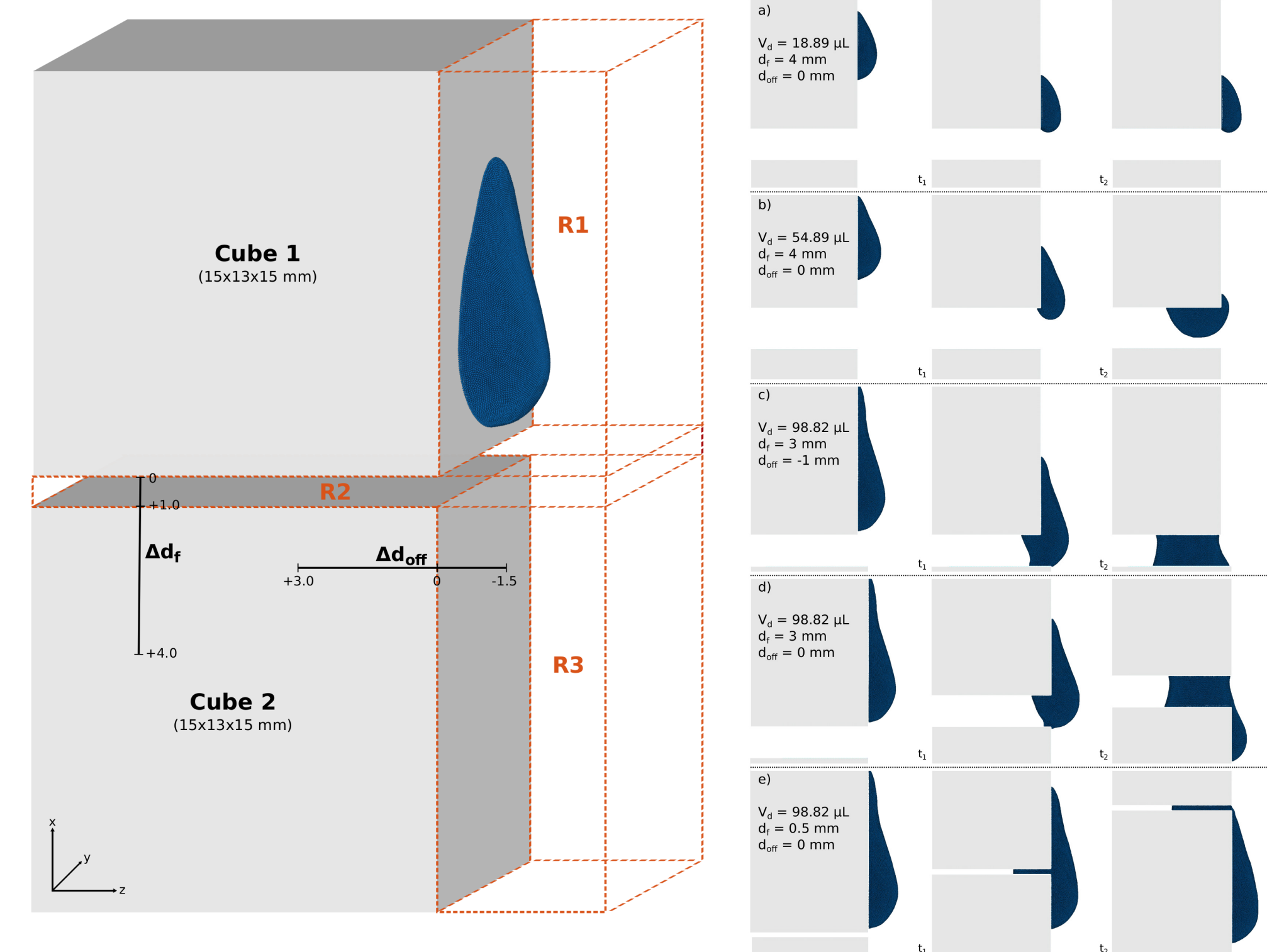


Figure 4: Morphology of the orthogonal fracture intersection in SPH.

Figure 5: Example cases. Time advances from left to right.

Influence of fracture geometry

- Positive ($54\mu\text{L} \leq V < 88\mu\text{L}$) and negative offsets inhibit vertical flow (fig. 7). Washburn-type fracture inflow occurs.
- Higher accumulation of water in the horizontal fracture domain with increasing aperture d_f ($V \geq 54\mu\text{L}$)(fig. 7).
- Small droplets ($V < 54$) may hydraulically connect to the lower horizontal fracture wall (when d_f is very small)

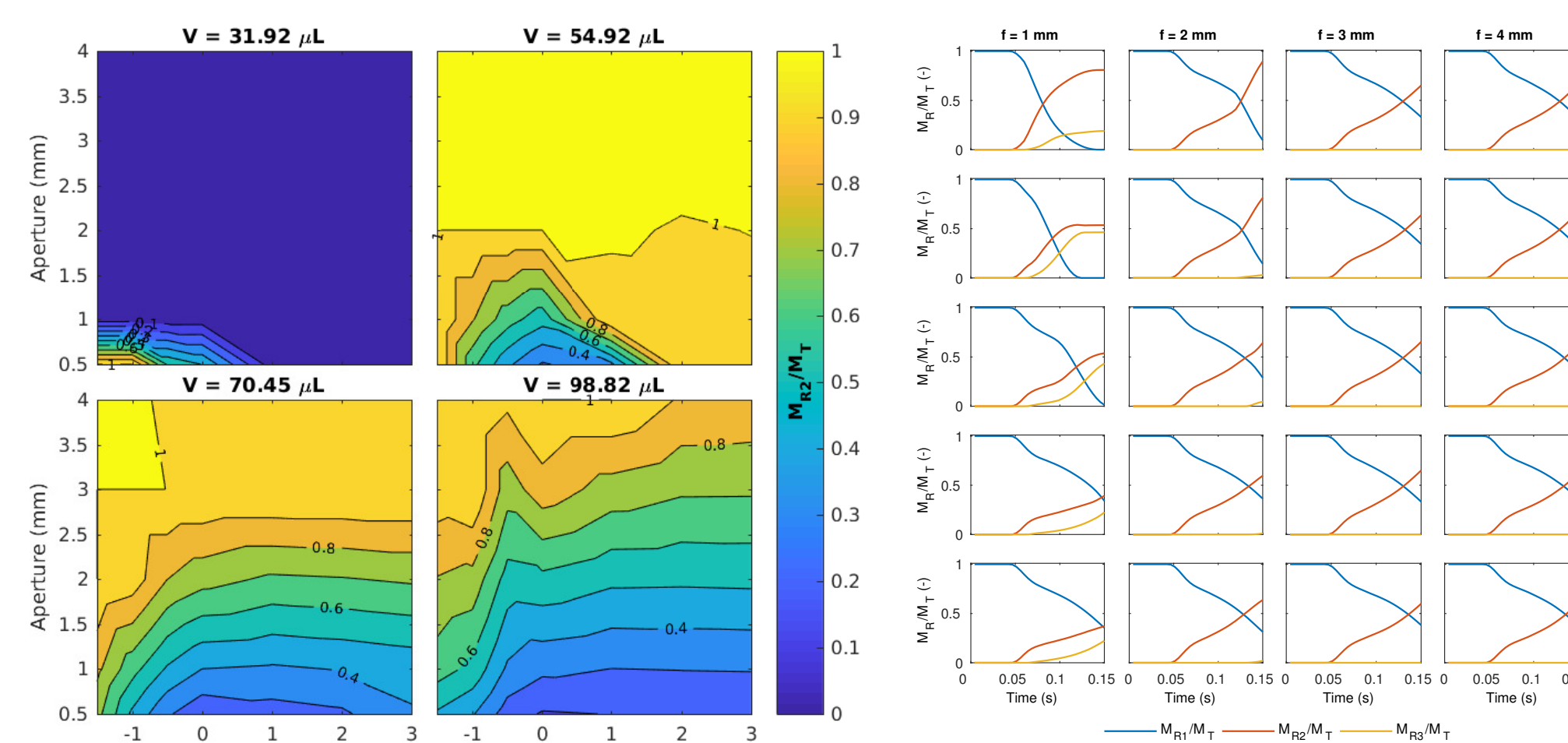


Figure 6: Total accumulated mass ratio of fluid in the horizontal fracture domain.

Influence of droplet volume and height

- With increasing droplet size, the influence of interfacial forces with respect to gravitational forces decreases. Therefore, the capillary force pinning the droplet onto the fracture surface is dominating the force balance for smaller droplets
- Below a certain Bond number $Bo \approx 1.8$ (Fig. 8), a droplet will remain pinned on the upper vertical fracture wall

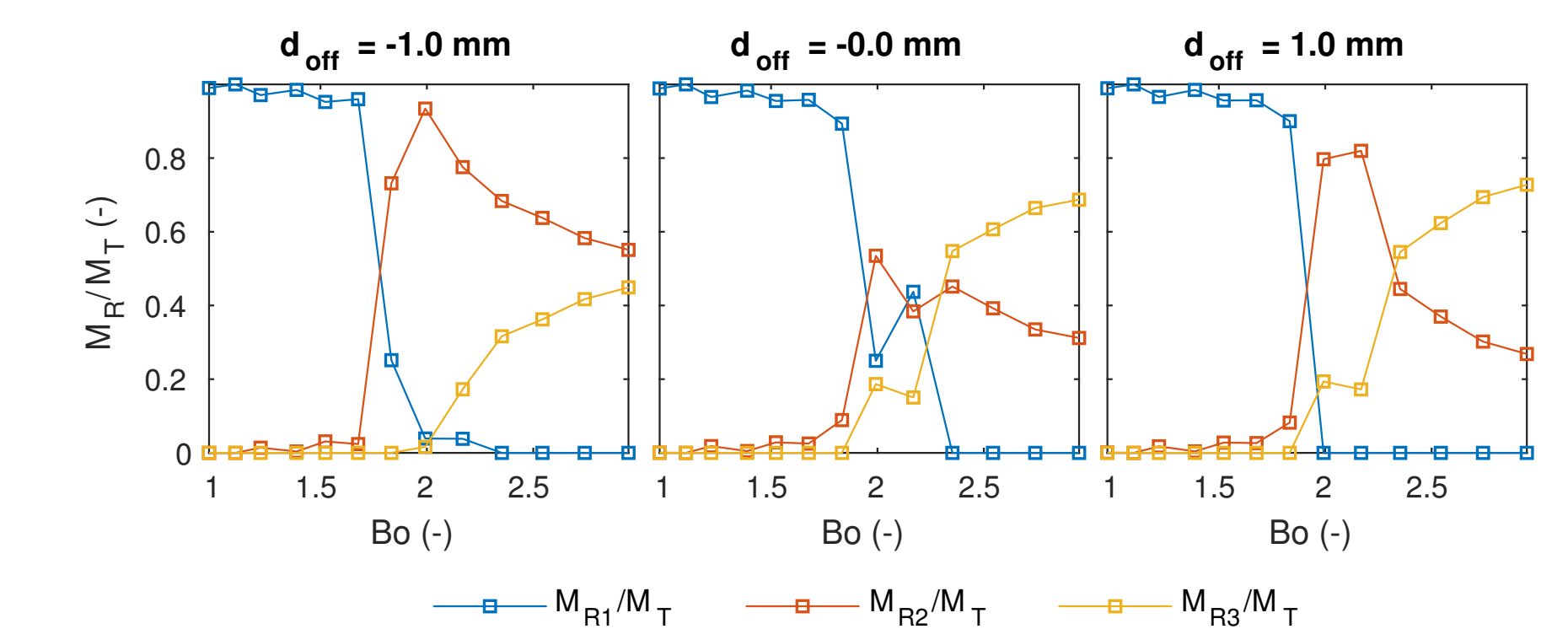


Figure 8: Mass ratio M_R/M_T in the domain R_1 , R_2 and R_3 with respect to the Bond number Bo . An aperture of $d_f = 1.0$ mm was applied.

- A linear dependence between the bypassing fluid mass and the ratio of droplet height and aperture d_f/h_d can be observed (fig. 9)

$$\frac{M_{R3}}{M_T} = \tau_1 \frac{d_f}{h_d} + \tau_2, \quad (7)$$

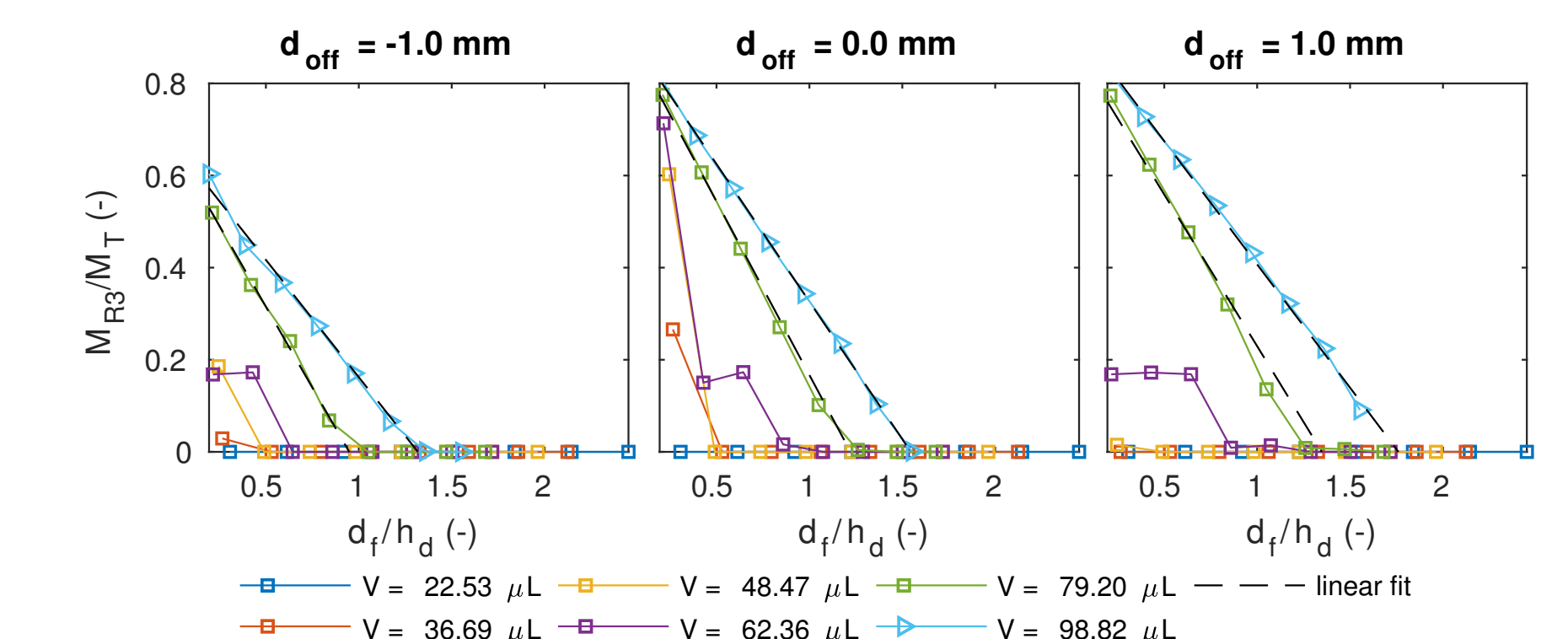


Figure 9: Mass ratio of the bypassing fluid with respect to aperture and droplet height d_f/h_d .

V. Conclusion & Outlook

Key Conclusions:

- A three-dimensional Pairwise-Force Smoothed Particle Hydrodynamics model was applied in order to simulate gravity-driven multiphase flow at synthetic fracture intersections
- Significant differences in fluid dynamics at fracture intersections could be observed when minor changes to the geometry of fracture intersection or droplet volume were implemented

Outlook

- Derive an analytical correlation and interpretation of partitioning dynamics, droplet height and aperture
- Establish transition thresholds in terms of Capillary and Bond number scalings (Podgorski, 2001) to understand long-term percolation dynamics of preferential flows (Kordilla et al. 2017)

Acknowledgement:

This work was funded by the Deutsche Forschungsgemeinschaft (DFG; German Research Foundation) under grant no. SA 501/26-1 and KO 53591/1-1.

References:

Kordilla (2017): Water Resour. Res. (Early View); Podgorski (2001): Phys. Rev. Lett. (87); Tartakovsky (2005): Phys. Rev. (72); Pan (2014): J. Comput. Phys (259)